Proceedings of the 9th International Conference on Structural Dynamics, EURODYN 2014
Porto, Portugal, 30 June - 2 July 2014
A. Cunha, E. Caetano, P. Ribeiro, G. Müller (eds.)
ISSN: 2311-9020; ISBN: 978-972-752-165-4

Model-based force identification in experimental ice-structure interaction by means of Kalman filtering

Torodd S. Nord[1], Eliz-Mari Lourens[2], Ole Øiseth[3], Andrei Metrikine[2]
[1] Sustainable Arctic Marine and Coastal Technology, Department of Civil Engineering, Norwegian University of Science and Technology, Trondheim, Norway.
[2] Faculty of Civil Engineering and Geosciences, Delft University of Technology, Delft, the Netherlands.
[3] Department of Structural Engineering, Norwegian University of Science and Technology, Trondheim, Norway.

email: Torodd.Nord@ntnu.no, E.Lourens@tudelft.nl, Ole.Oiseth@ntnu.no, A.Metrikine@tudelft.nl

ABSTRACT: The level-ice forces exerted on a scale model of a compliant bottom founded structure are identified from non-collocated strain and acceleration measurements by means of a joint input-state estimation algorithm. The identification is performed based on two different finite element models: one entirely based on the blueprints of the structure, and an updated one which predicts the first natural frequency more accurately. Results are presented for two different excitation scenarios characterized by the ice failure process and ice velocity, and known as the intermittent crushing and the continuous brittle crushing regimes. The accuracy of the identified forces is assessed by comparing them with those obtained by a frequency domain deconvolution on the basis of experimentally obtained frequency response functions. Results show a successful identification of the level-ice forces for both the intermittent and continuous brittle crushing regimes, even when significant modeling errors are present. The ice-induced displacements of the structure identified in conjunction with the forces are also compared to those measured during the experiment. These are found to be sensitive to the modelling errors in the blueprint model. By a simple tuning of the model, however, the estimated response is seen to match the measured one with high accuracy.

KEY WORDS: Dynamic ice-structure interaction; inverse problems; Kalman filtering; force identification.

1 INTRODUCTION

Level-ice forces have been measured on bottom-founded structures since the very first oilplatforms in the Cook Inlet, Alaska [1]. The action of the level-ice on the platforms induced severe vibrations, on some occasions threatening the structural integrity. The Molikpaq platform was deployed at different sites in the Canadian Beufort Sea in the 1980's. The platform was equipped with data acquisition systems for measuring ice forces and deformations of the structure. The measured ice forces from the so-called MEDOF panels have been widely used since then, but also questioned for their operational accuracy and reliability, reviewed by e.g. Frederking et al., Jefferies et al. and Spencer [2-4].

Force identification by means of frequency domain deconvolution was performed by Montgomery and Lipsett [5] to study the river-ice forces on the bridge crossing the Athabaska river in Alberta, Canada. They identified the forces using a frequency response function (FRF) from a single-degree-of-freedom model and measured structural response. Määttänen [6] applied the same method to identify the ice forces on a lighthouse in the Gulf of Bothnia. An ice-breaker vessel connected by a wire to the lighthouse was used to perform a step relaxation test ([7]) in order to obtain the FRF from the measured excitation and response. Unfortunately, a poor coherence function was found, such that the ice forces had to be identified using a FRF from modal decomposition instead. Määttänen [8] identified the ice forces using the experimentally obtained FRF in a later publication. The accuracy of the frequency domain deconvolution approach has been questioned by Timco et al. [9] and Singh et al. [10] where attention was drawn to the fact that the identified ice forces were overestimated compared to the directly measured forces in regimes where the response was close to the natural frequency of the structure. In order to reduce the difference between the identified and measured forces they suggested to increase the damping in the dynamic model. Fabumni [11] studied the number of forces that can be identified at a specific frequency dependending on the number of participating modes at that frequency. In the special case when only one mode is contributing in the response signal around the natural frequency, Fabumni demonstrated that only one force can be reconstructed with acceptable accuracy.

The harsh environment affects the ability to deploy sensors on arctic offshore structures. Unless the inner surface of the structure can be accessed, the ice-action point may be a challenging location to install a sensor since the ice is crushing on the outer surface of the structure. This implies that non-collocated sensors may be the only realistic option. Hollandsworth [12] demonstrated the significance of sensor collocation, and found that if the sensors were deployed far from the excitation point, the forces were likely to be underestimated. Water level fluctuations or rafting of the ice cause variations in the location of the ice-action point on bottom-founded structures. This implies that perfect collocation of the sensors is in practice difficult to achieve.

Identification accuracy does not only depend on the sensor locations or modeling errors, since the structural design of the experiment, calibration procedures and noise levels may prevail. When using direct ice-force measurements, the internal damping and natural frequencies of the load panels or load cells must be treated carefully, as they may interfere with the ice-failure. Whenever the directly measured force signals include inertia from the measurement setup itself, subtraction of the undesired inertia is required to attain the ice force (Barker et al.[13]).

Another instrument that can be used to obtain the ice forces is the tactile sensors (e.g. [14]-[15]). These sensors have the advantage that they can measure pressure with a high spatial resolution and that they can be tailored to fit any indenter and enable extraction of both contact area and pressure. However, the sensors can only measure stresses normal to the surface of the indenter, so that any shear stresses have to be derived through assumed static and dynamic friction coefficients. So far the application of the tactile sensor has been limited to small and medium scale experiments.

Ice forces have traditionally been obtained by either direct force measurements or deterministic force identification in the frequency domain. A disadvantage of the latter method is that it is often problematic to accurately determine the FRFs of large structures. Since the offshore structures deployed in the arctic are not an exception, in situ ice forces are difficult to obtain from frequency domain deconvolution and output only measurements. Direct measurement, on the other hand, implies heavy costs related to the load panels, installation and maintenance. Response measurements are therefore still favorable as a means to obtain the forces. Additionally, they provide important information about the structural motion.

In this contribution, we demonstrate a methodology to overcome the aforementioned difficulties. A recently developed combined deterministic-stochastic approach is used to jointly identify the ice forces and the states. The original algorithm was proposed by Gillijns and De Moor [16], and was intended for use in the field of optimal control. Lourens et al. [17] extended the algorithm for use with reduced-order systems, as often encountered in structural dynamics. Niu et al. [18] used the original algorithm to identify forces on a laboratory scale structure. The deterministic-stochastic nature of the algorithm allows for improved results when the model equations are inexact. Since the algorithm requires no regularization, it can be applied online.

In what follows, the ice forces are identified in conjunction with the states using the original algorithm [16] and a limited number of response measurements on a laboratory test setup designed for ice-induced vibrations. The results are assessed by comparison with the forces obtained with frequency domain deconvolution, and the estimated displacements are compared with the ones measured.

2 FUNDAMENTALS

2.1 System equations

The governing equations of motion for a linear system discretized in space and excited by an external force, can be written as follows:

$$M\ddot{u}(t)+C\dot{u}(t)+Ku(t)=f(t)=S_p p(t) \tag{1}$$

where $u\in\mathbf{R}^{n_{DOF}}$ is the displacement vector, and the matrices $M,C,K\in\mathbf{R}^{n_{DOF}\times n_{DOF}}$ denote the structural mass, damping and stiffness matrix, respectively. The excitation vector $p(t)\in\mathbf{R}^{n_p}$ is acting on the desired locations through the force influence matrix $S_p\in\mathbf{R}^{n_{DOF}\times n_p}$, where n_p is the number of force time histories.

2.2 State-space description

The continuous time state vector $x(t)\in\mathbf{R}^{n_s}$, $n_s=2n_{DOF}$ is defined as:

$$x(t)=\begin{pmatrix}u(t)\\ \dot{u}(t)\end{pmatrix} \tag{2}$$

and the equation of motion of second order, Eq.(1), can be re-written as a first-order continuous-time state equation

$$\dot{x}(t)=A_c x(t)+B_c p(t) \tag{3}$$

where the system matrices $A_c\in\mathbf{R}^{n_s\times n_s}$ and $B_c\in\mathbf{R}^{n_s\times n_p}$ are defined as

$$A_c=\begin{bmatrix}0 & I\\ -M^{-1}K & -M^{-1}C\end{bmatrix}, B_c=\begin{bmatrix}0\\ M^{-1}S_p\end{bmatrix} \tag{4}$$

The measurements are arranged in a data vector $d(t)\in\mathbf{R}^{n_d}$, in which the observations can be a linear combination of displacement, velocity and acceleration, with n_d the number of data measurements. The data vector is constructed as follows:

$$d(t)=S_a\ddot{u}(t)+S_v\dot{u}(t)+S_d u(t) \tag{5}$$

where the selection matrices S_a, S_v and $S_d\in\mathbf{R}^{n_d\times n_{DOF}}$ are populated according to the spatial location where acceleration, velocity and/or displacement are measured. By premultiplying Eq. (1) with M^{-1}, inserting the resulting expression into Eq. (5), and further utilizing the definition of the state vector, Eq.(5) can be transformed to the state-space formulation:

$$d(t)=G_c x(t)+J_c p(t) \tag{6}$$

where the matrices $G_c\in\mathbf{R}^{n_d\times n_s}$ and $J_c\in\mathbf{R}^{n_d\times n_p}$ represent the output influence matrix and direct transmission matrix, respectively, defined as:

$$G_c=[S_d-S_aM^{-1}K \quad S_v-S_aM^{-1}C],\ J_c=[S_aM^{-1}S_p]$$

In discrete time under a zero-order hold assumption and given a sampling rate of $1/\Delta t$, Eqs. (3) and (6) can be defined as follows:

$$x_{k+1}=Ax_k+Bp_k \tag{7}$$

$$d_k=Gx_k+Jp_k \tag{8}$$

where

$$x_k=x(k\Delta t),\ d_k=d(k\Delta t),\ p_k=p(k\Delta t),\ k=1,\ldots,N$$

and

$$A=e^{A_c\Delta t},\ B=[A-I]A_c^{-1}B_c$$
$$G_c=G,\ J_c=J$$

2.3 Joint input-state estimation algorithm

Assuming the system matrices known, the algorithm developed by Gilljins and De Moor [16] is used to jointly

estimate the forces and states. By introducing random variables w_k and v_k representing the stochastic system and measurement noise, respectively, the discrete-time state-space equations become

$$x_{k+1} = Ax_k + Bp_k + w_k \tag{9}$$

$$d_k = Gx_k + Jp_k + v_k \tag{10}$$

where it is assumed that the vectors w_k and v_k are mutually uncorrelated, zero-mean, white noise signals with known covariance matrices $Q = E\{w_k w_l\} \geq 0$ and $R = E\{v_k v_l\} > 0$. The algorithm predicts the force and state in three steps: the unbiased minimum-variance input estimation (MVU), the measurement update and the time update.

Input estimation:

$$\tilde{R}_k = GP_{k|k-1}G^T + R \tag{11}$$

$$\mathcal{M}_k = (J^T \tilde{R}_k^{-1} J)^{-1} J^T \tilde{R}_k^{-1} \tag{12}$$

$$\hat{p}_{k|k} = \mathcal{M}_k (d_k - G\hat{x}_{k|k-1}) \tag{13}$$

$$P_{p[k|k]} = (J^T \tilde{R}_k^{-1} J)^{-1} \tag{14}$$

Measurement update:

$$L_k = P_{k|k-1} G^T \tilde{R}_k^{-1} \tag{15}$$

$$\hat{x}_{k|k} = \hat{x}_{k|k-1} + L_k (d_k - G\hat{x}_{k|k-1} - Jp_{k|k}) \tag{16}$$

$$P_{k|k} = P_{k|k-1} - L_k (\tilde{R}_k - J\ P_{p[k|k]} J^T) L_k^T \tag{17}$$

$$P_{xp[k|k]} = P_{px[k|k]}^T = -L_k J\ P_{p[k|k]} \tag{18}$$

Time update:

$$x_{k+1|k} = A\hat{x}_{k|k} + B\hat{p}_{k|k} \tag{19}$$

$$P_{k+1|k} = \begin{bmatrix} A & B \end{bmatrix} \begin{bmatrix} P_{k|k} & P_{xp[k|k]} \\ P_{px[k|k]} & P_{p[k|k]} \end{bmatrix} \begin{bmatrix} A^T \\ B^T \end{bmatrix} + Q \tag{20}$$

For more details on the algorithm and the assumptions it is based upon, the reader is referred to [16].

3 EXPERIMENTAL

The force identification algorithm outlined above is applied to data from the *Deciphering Ice-Induced Vibration* test campaign at the Hamburg Ice Basin HSVA, carried out in 2011. See Määttänen et al. [19], Hendrikse et al. [20] and Nord and Määttänen [21] for further details. One test from that campaign, referred to as test 4300, is used in this study. The main components of the experimental setup are shown in figure 1. The ice sheet was floating on water and the compliant test structure was fixed to a carriage. During testing the carriage forced the structure through the ice sheet causing continuous ice failure at the indenter. The carriage velocity (ice velocity) was changed in order to investigate the different crushing regimes governing the interaction.

3.1 Test structure

The structure was designed to have a nominal scale ratio of 1:8-1:10 to a generic bottom-founded offshore structure. The structure was scaled to achieve modal similitude, meaning that the natural modes of the laboratory structure resemble the full-scale natural modes. More about the dynamic scaling can be found in Määttänen et al. [19]. The first two natural modes have large amplitudes at the ice-action level. The frequency of vibration was expected to change from the first to the second natural frequency with increasing ice velocity.

To make the structure flexible the main beam was supported by two leaf springs attached to the two vertical support beams displayed in yellow in figure 1. The flexibility of the system could then be adjusted by changing the spacing between the vertical supports. To be able to further tune the system towards the desired natural frequencies the disc weights displayed in green in figure 1 could be added to the bottom and top of the structure. The bracings and joints were designed to retain low internal friction in order to avoid nonlinearities and to maintain a low structural damping. At the location of the ice action, a cylindrical indenter with a 220mm diameter was attached to the main shaft.

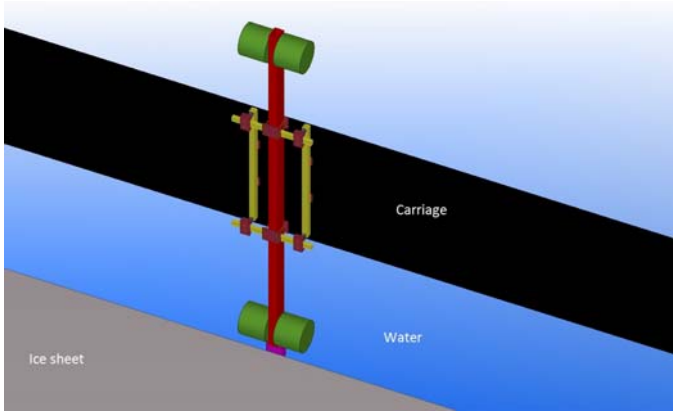

Figure 1: Overview of the test setup. The compliant structure was mounted to the carriage that forced the structure through the ice sheet.

3.2 Sensoring and data acquisition

All sensors were located on the lower part of the structure (figure 2). The accelerometer was installed close to the indenter, while the strain gauge was attached to the main beam approximately 750mm above the ice-action point. Two laser displacement sensors were installed on a separate frame to monitor the structural displacements at the lower part of the beam. The load cell installed at the ice-action point was only used to access the dynamic properties of the structure before it was subjected to ice forces. The data was sampled at 100Hz.

3.3 Dynamic calibrations

A step relaxation test in open water prior to each ice test provided the static and dynamic properties of the structure [7]. A steel rod connected to the structure at the ice-action level was gradually loaded using a jack. Between the rod and the ice-action point a weak link was installed, which failed at a selected load level, causing transient vibrations. From the measured excitation and response, the FRF was calculated. Note that an active load cell was installed only during the

dynamic calibrations, and not during ice action. Direct ice-force measurements would require a more complex structure design with a comprehensive installation and calibration. Therefore the frequency domain deconvolution method based on the experimentally obtained FRFs was used to reconstruct the ice forces (see section 5.2). At least one calibration test was performed for each structural configuration. In test 4300, the first and second natural frequencies were identified to be 12.2 and 16.2 Hz.

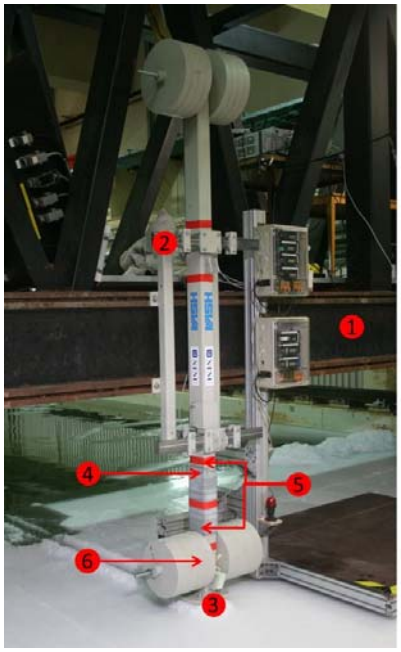

Figure 2. Test-setup overview, photo from ice-testing.

3.3 Ice-sheet properties

The ice properties are important for the repeated ice failure, hence influencing the characteristics of the dynamic response. The tests were carried out in the 78 m long and 10 m wide HSVA Large Ice Tank. The water depth is 2.5 m with a deep section of 5 m at the end of the basin (10 × 12 m). The ice sheets were columnar-grained, produced in NaCl-doped water with a salinity of 6.8‰ by seeding. The crystal size was controlled by scraping the ice from underneath. Gas bubbles were embedded in the growing ice sheet to ensure the brittle behavior of the ice as described by Määttänen et al. [19] and Evers and Jochmann [22]. Subsequent to the ice growth process at -22°C, the temperature was raised to hit the target ice properties. Test 4300 had relatively warm ice, hence the uniaxial compressive and flexural strength values were low. The governing ice parameters can be found in Nord et al.[23].

4 FE MODEL AND STRAIN OBSERVATIONS

4.1 FE Model

To obtain the system matrices A, B, G and J the structural properties in terms of the global M , C and K matrices must be known. These matrices can be obtained by discretization using the finite element method. The FE model of the structure used in this work is displayed in Figure 3. The structure is modeled as a beam supported by two linear springs. 43 Beam elements with 6 DOFs in each node are used for the hollow-section (RHS120x80x6) profile main beam, while the additional mass of the structure at discrete locations is modelled using lumped masses.

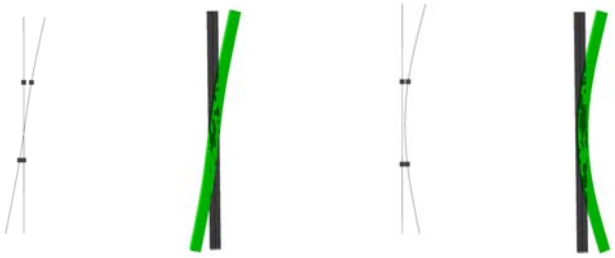

Figure 3. FE-model showing the spring locations, side view of beam profile and vibration modes. The first and second modes are displayed in the left and right figure, respectively.

First, a model based only on structural blueprints is used in the identification to assess how well the force can be reconstructed without any prior knowledge of the true (measured) dynamical properties. Secondly, a tuned model is assembled based on the knowledge obtained from the dynamic calibrations. The FE software was used to derive the M and K matrices while Rayleigh damping is used to construct the damping matrix.

Model based on structural blueprints

The stiffness of the linear springs is the combined stiffness of the vertical support beams and the leaf springs, where the combined stiffness relies on the accuracy of the simplistic beam formulas used for the structural design. The added masses from the weight discs were 120kg in top and bottom, while the indenter and foundation masses were 32kg and 15kg, respectively. The design was intended to provide low internal damping, so that Rayleigh damping coefficients are calculated based on an assumed damping ratio of 2% in the first and second modes.

Model tuned using dynamic calibration data

The modeling errors are assumed to originate mainly in the foundation. The boundary conditions used in the design calculation of the combined stiffness rendered a smaller stiffness than observed. As a consequence, the tuning solely affects the model springs. The stiffness is tuned until the first natural frequency is close to the one found in the receptance plot from the dynamic calibrations. This limited amount of tuning parameters is considered to be favorable for the comparative results presented in section 5. The structural properties for both the blueprint and the tuned model are given in Table 1.

Table 1. FE model properties

Property	Lower Spring stiffness	Upper Spring stiffness	Natural Frequencies		Damping Ratios		Rayleigh coefficients	
symbol	k_L [kN/m]	k_U [kN/m]	f_1 [Hz]	f_2 [Hz]	ζ_1 [%]	ζ_2 [%]	α	β
Blueprint model	7.10	4.62	11.17	16.84	2.0	2.0	1.68	2.27e-4
Tuned model	8.84	5.61	12.12	17.34	2.0	2.0	1.79	2.16e-4

4.2 Strain observations

In order to use the measured strain data to identify the forces and states, the strains must be described through the linear relationship between the output influence matrix, *G*, and the states. When the shape functions used to establish the finite element are known, they can be readily used to establish the complete transformation from (predicted) states to strain. A two-node beam element has been used in this work. The element has six degrees of freedom (directions illustrated in Figure 4) in each node and shear deformations have been taken into account - see [24] and [25] for further details.

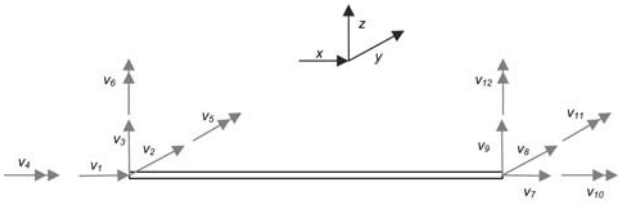

Figure 4. Beam element directions.

The general relation between the transverse displacement field and the generalized degrees of freedom can be written as follows:

$$w(x) = N_q q \tag{21}$$

where $N_q = [1 \quad x \quad x^2 \quad x^3]$ and $q = A_{el}^{-1} v$ are the generalized displacement patterns and the generalized DOFs, while v symbolizes the physical element DOFs. The A_{el} matrix must be given for deformations in both *xz* and *xy* planes. For lateral motion in the y direction and rotation about the z axis (*xy* plane), the matrix A_{el} is the following:

$$v = A_{el} q, \begin{bmatrix} v_2 \\ v_6 \\ v_8 \\ v_{12} \end{bmatrix} = \begin{bmatrix} w(0) \\ -w_{,x}(0) - \frac{\alpha L^2}{12} w_{,xxx}(0) \\ w(L) \\ -w_{,x}(L) - \frac{\alpha L^2}{12} w_{,xxx}(L) \end{bmatrix} = \begin{bmatrix} 1 & 0 & 0 & 0 \\ 0 & -1 & 0 & \frac{-\alpha L^2}{2} \\ 1 & L & L^2 & L^3 \\ 0 & -1 & -2L & \frac{-L^2(6+\alpha)}{2} \end{bmatrix} q \tag{22}$$

where α is the dimensionless shear coefficient given in [24]. Inserting the expression for the generalized DOFs into Eq. (22), the element shape functions are obtained as follows:

$$w_y(x) = N_q q = N_q A_{el}^{-1} v = N^{el} v \tag{23}$$

When the shape-functions N^{el} are given through the relation in Eq. (24), the bending strain can be found as:

$$\begin{aligned} \varepsilon_b(x) &= -y w_{y,xx} = -y N^{el}_{y,xx} v = \\ -y \Bigg[& -\frac{6}{L^2(1+\alpha)} + \frac{12x}{L^3(1+\alpha)} \quad -\frac{4+\alpha}{L(1+\alpha)} + \frac{6x}{L^2(1+\alpha)} \\ & \frac{6}{L^2(1+\alpha)} - \frac{12x}{L^3(1+\alpha)} \quad -\frac{2+\alpha}{L(1+\alpha)} + \frac{6x}{L^2(1+\alpha)} \Bigg] v \end{aligned} \tag{24}$$

where y is the distance from the center of inertia to the point on the cross-section where the strain is measured. Since the strains are not continuous between the elements, the bending strain at the node of interest can be taken as the average over two neighboring elements. The data influence matrix for strain (see equation (5)), denoted S_d, has to be populated according to the global DOF vector u.

5 RESULTS AND DISCUSSION

5.1 Observations

The ice velocity (recorded carriage velocity) was increased in steps, ranging from 10 to 300 mm/s. At low velocities the ice followed the deflection of the structure with a ductile load build up and a subsequent spring-back deflection due to brittle failure. These response characteristics were only observed for a few seconds; thereafter the failure process alternated between intermittent and continuous brittle crushing. Underwater cameras revealed that the extrusion of crushed ice primarily consisted of small particles with some larger pieces spalling off. Radial cracks were occasionally observed, but they did not expand to the walls of the ice tank.

5.2 Reference force

The FRF was obtained experimentally from the step-relaxation test as described in section 3. The ice force used for validation was subsequently found by inverting the FRF as follows:

$$\hat{\mathrm{p}}(\omega) = \hat{\mathrm{H}}^{\dagger}(\omega)\ \hat{\mathrm{d}}(\omega) \tag{25}$$

where $\hat{\mathrm{p}} \in \mathbf{R}^{n_p}$ is the force, $\hat{\mathrm{d}} \in \mathbf{R}^{n_d}$ is the measured response and $\hat{\mathrm{H}}^{\dagger} \in \mathbf{R}^{n_d \times n_p}$ is the pseudo-inverse of the FRF matrix. A more detailed description of this procedure can be found in Nord et al. [23]. In what follows, the forces obtained using the measured FRF will be referred to as the reference force.

5.3 Force identification

The ice force and the states are identified on the basis of one strain gauge and one accelerometer, both non-collocated as shown in Figure 2. The values assigned to the diagonals of the covariance matrices $Q, R, P_{0|-1}$ required by the joint input-state estimator (section 2.3), namely $10e^{-8}$, $10e^{-6}$, and $10e^{-8}$, are chosen based on the peaks in the measured response and the identified states, see [17] for details. The initial state $\hat{x}_{0|-1}$ is assigned the value of 0, effectively treating it as an unknown.

Blueprint model

The identified force appears almost identical to the reference force (figure 5), with the only discrepancy observed at the very end of the test. In order to investigate whether the algorithm and an approximate model are able to reconstruct

the forces in the two fundamental ice-crushing regimes, two short sequences representing each of these regimes are selected. The results for the intermittent crushing regime are shown in figure 6. The identified force exhibits the classical saw-tooth behavior of intermittent crushing, as each cycle appears almost identical to the reference force. The corresponding Fourier spectrum is shown in figure 7. In the more dynamic, continuous crushing regime (Figure 8), the force is also identified accurately. Only at higher frequencies (see figure 9), the difference becomes slightly more pronounced. In general, the convincing agreement between the reference force and the force identified based on an approximate blueprint model, provides a strong motivation for using the joint-input state algorithm for in-situ full-scale ice-force identification.

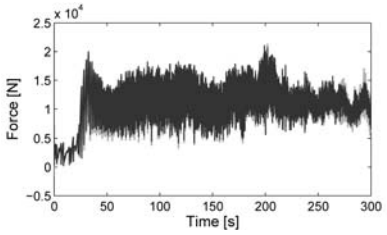

Figure 5. Identified force (light grey) and reference force (black) for the blueprint model.

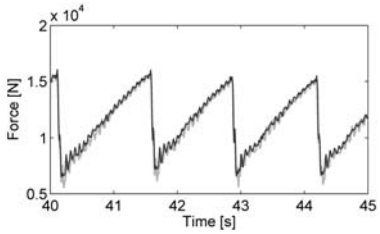

Figure 6. Identified (light grey) and reference force (black) for the blueprint model in intermittent crushing.

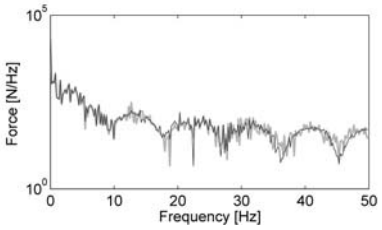

Figure 7. Frequency spectra of the identified (light grey) and reference force (black) for the blueprint model in intermittent crushing.

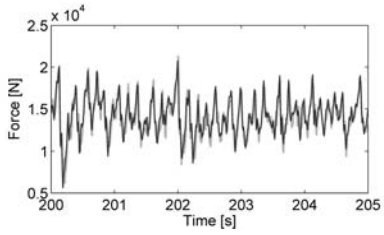

Figure 8. Identified (light grey) and reference force (black) for the blueprint model in continuous crushing.

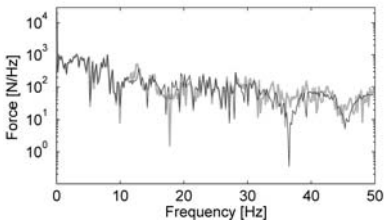

Figure 9. Frequency spectra of identified (light grey) and reference force (black) for the blueprint model in continuous crushing.

Tuned model

Figure 10 shows an overall excellent reconstruction of the forces based on the tuned model. The improvements can be spotted in the peaks and valleys in figure 11 (cf. figure 8), Where a small discrepancy is observed at the end of the time series for the blueprint model (figure 5), it is now almost absent in the tuned model (figure 10).

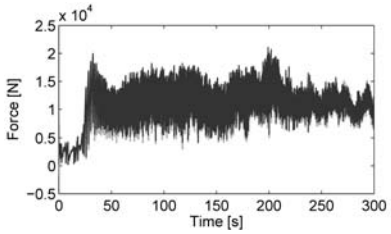

Figure 10. Identified force (light grey) and reference force (black) for the tuned model.

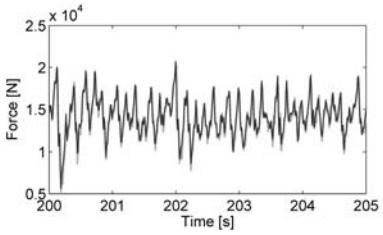

Figure 11. Short sequence of brittle crushing, identified (light grey) and reference force (black) for the tuned model.

5.4 Response estimation

While the foregoing application of the algorithm focused on the identification of the forces, here the aim is to show the accuracy of the (jointly) estimated displacement at unmeasured locations. Recall that, in what follows, only the non-collocated acceleration and strain gauge are used to estimate the displacement at the location of the lowermost laser.

Blueprint model

The measured and estimated displacements are displayed in figure 12. The displacements are overestimated throughout the test. In the intermittent crushing regime (figure 13) the peak offsets remain constant, while for the continous crushing regime (figure 15), some peaks differ less than others. The shape of each cycle is well captured for the intermittent regime, while for the brittle crushing regime the load build up phase differs prior to the terminal ice failure. Still, the frequency plots in figure 14 and figure 16 show that the

dominant frequency components are in good agreement with the measurements. Since the significant modeling errors for this test setup pertain to the foundation stiffness, their effect influences mostly the state prediction, while acceptable force identification accuracy was preserved.

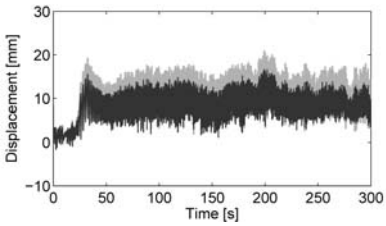

Figure 12. Estimated displacement (light grey) and the measured (black).

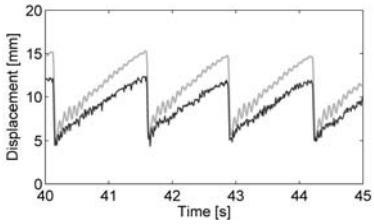

Figure 13. Estimated displacement (light grey) and the measured (black) in intermittent crushing.

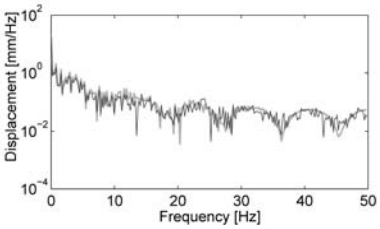

Figure 14. Estimated displacement (light grey) and the measured (black) in intermittent crushing, frequency domain.

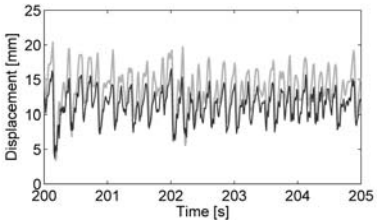

Figure 15. Estimated displacement (light grey) and the measured (black) in continuous brittle crushing.

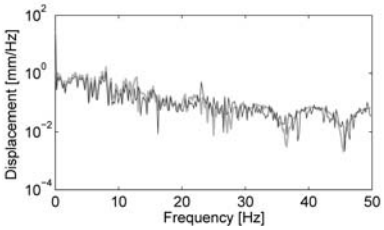

Figure 16. Estimated displacement (light grey) and the measured (black) in continuous brittle crushing.

Tuned Model

The overall agreement between measured and estimated response (figure 17) improves significantly when tuning the foundation stiffness. The constant peak offset in the intermittent regime (figure 18) reduces to 1mm, while in continuous crushing (figure 20) the difference ranges from 0 to 2mm. Reducing the peak offset for intermittent crushing has limited effect on the higher frequencies displayed in figure 19. The improved accuracy is as expected more visible in the frequency domain during continuous crushing (figure 21). The light grey and dark lines follow each other well and the major frequency components are well captured.

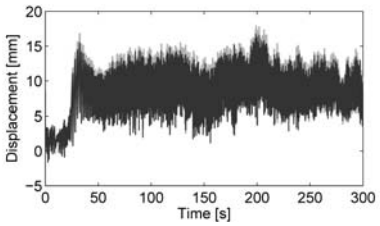

Figure 17. Estimated displacement (light grey) and the measured (black).

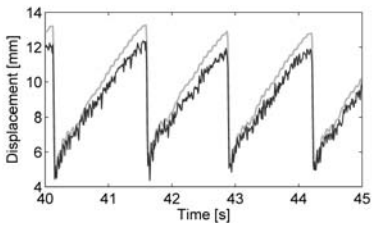

Figure 18. Estimated displacement (light grey) and the measured (black) in intermittent crushing.

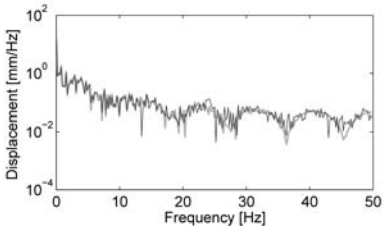

Figure 19. Estimated displacement (light grey) and the measured (black) in intermittent crushing, frequency domain.

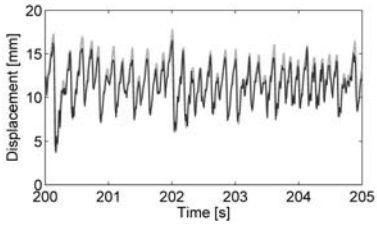

Figure 20. Estimated displacement (light grey) and the measured (black) in continuous brittle crushing.

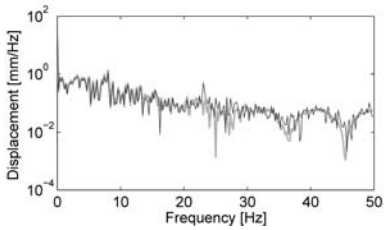

Figure 21. Estimated displacement (light grey) and the measured (black) in continuous brittle crushing, frequency domain.

6 CONCLUSIONS

The ice forces acting a generic bottom-founded offshore structure have successfully been identified in conjunction with the states using a joint input-state algorithm and a limited number of response measurements. The ice forces are well reconstructed in two important regimes governing the dynamic ice-structure interaction. The estimated response is found to be prone to modelling errors, while excellent force identification results are obtained even with an approximate model. Simple tuning of the model foundation stiffness greatly improved the estimated response at the ice-action level. The results shown in this contribution provide a strong motivation for monitoring of full-scale structures in the Arctic region.

ACKNOWLEDGMENTS

The authors wish to acknowledge the support of the Research Council of Norway through the Centre for Research-based Innovation SAMCoT, and the support from all SAMCoT partners. The work described in this paper was supported by the European Community's 7th Framework Program through the grant to the budget of the Integrated Infrastructure Initiative HYDRALAB-IV, Contract no. 261520. The authors would like to thank the Hamburg Ship Model Basin (HSVA), especially the ice tank crew, for the hospitality, technical and scientific support and the professional execution of the test program in the Research Infrastructure ARCTECLAB.
In addition the authors are grateful for the Finite Element support from Associate Professor Bjørn Haugen at the Department of Engineering Design and Materials at the Norwegian University of Science and Technology.

REFERENCES

[1] Peyton, H.R., *Sea Ice Strength*, in *Report UAG-182 from Geophysical Institute, University of Alaska*. 1966, Office of Naval research.
[2] Frederking, R., et al., *ICE LOAD MEASURING PANELS – THE NEXT GENERATION*, in *IAHR*. 2002: New Zealand. p. 450-457.
[3] Jefferies, M., et al., *Ice Load Measurement on Molikpaq: Methodology and Accuracy*, in *Port and Ocean Engineering under Arctic Conditions*. 2011: Montréal, Canada.
[4] Spencer, P., *A review of the MEDOF panels installed on the Molikpaq structure in the Canadian Beaufort sea*, in *International Conference on Port and Ocean Engineering under Arctic Conditions (POAC)*. 2013: Espoo, Finland.
[5] Montgomery, C.J. and A.W. Lipsett, *ESTIMATION OF ICE FORCES FROM DYNAMIC RESPONSE*, in *International Symposium on Ice (IAHR)*. 1981: Quebec, P.Q. Canada. p. 771-782.
[6] Määttänen, M., *True ice force by deconvolution*, in *1st International Modal Analysis Conference (IMAC)*. 1982: Orlando, FL, USA. p. 556-590.
[7] Ewins, D.J., *Modal Testing: Theory, Practice and Application*. Vol. Second Edition. 2000.
[8] Määttänen, M., *DYNAMIC ICE-STRUCTURE INTERACTION DURING CONTINOUS CRUSHING*, in *U.S. Army Cold Regions Research and Engineering Laboratory, Hanover, NH 03755. CRREL Report 83-5*. 1983.
[9] Timco, G.W., R. Frederking, and S.K. Singh. *THE TRANSFER FUNCTION APPROACH FOR A STRUCTURE SUBJECTED TO ICE CRUSHING*. in *POAC*. 1989. Luleå, Sweden.
[10] Singh, S.K., et al., *TESTS OF ICE CRUSHING ON A FLEXIBLE STRUCTURE*, in *OMAE* 1990: Houston TX. USA. p. 89-94.
[11] Fabumni, J.A., *Effects of structural modes on vibratory force determination by the pseudoinverse technique.* AIAA Journal, 1986. **24**(3): p. 504-509.
[12] Hollandsworth, P.E. and H.R. Busby, *Impact force identification using the general inverse technique.* International Journal of Impact Engineering, 1989. **8**(4): p. 315-322.
[13] Barker, A., et al., *Ice loading on Danish wind turbines: Part 1: Dynamic model tests.* Cold Regions Science and Technology, 2005. **41**(1): p. 1-23.
[14] Sodhi, D. and R. Haehnel, *Crushing Ice Forces on Structures.* Journal of Cold Regions Engineering, 2003. **17**(4): p. 153-170.
[15] Määttänen, M., et al., *Ice crushing tests with variable structural flexibility.* Cold Regions Science and Technology, 2011. **67**(3): p. 120-128.
[16] Gillijns, S. and B. De Moor, *Unbiased minimum-variance input and state estimation for linear discrete-time systems with direct feedthrough.* Automatica, 2007. **43**(5): p. 934-937.
[17] Lourens, E., et al., *Joint input-response estimation for structural systems based on reduced-order models and vibration data from a limited number of sensors.* Mechanical Systems and Signal Processing, 2012. **29**(0): p. 310-327.
[18] Y.Niu, M.Klinkov, and C.-P. Fritzen. *Online force reconstruction using an unknown-input Kalman filter approach*. in *International Conference on Structural Dynamics, Eurodyn 2011*. 2011. Leuven, Belgium.
[19] Määttänen, M., et al., *Novel ice induced vibration testing in a large-scale facility*, in *"Ice Research for a Sustainable Environment"(IAHR)*. 2012: Dalian, China.
[20] Hendrikse, H., A. Metrikine, and K.-U. Evers, *A method to measure the added mass and added damping in dynamic ice-structure interaction:*, in *"Ice Research for a Sustainable Environment"(IAHR). Dalian, China.* 2012.
[21] Nord, T.S. and M. Määttänen. *Modal analysis in ice structure interaction*. in *IAHR*. 2012. Dalian, China.
[22] Evers, K.-U. and P. Jochmann. *An advanced tehnique to improve the mechanical properties of model ice developed at the HSVA ice tank*. in *Port and Ocean Engineering under Arctic Conditions*. 1993. Hamburg, Germany.
[23] Nord, T.S., M.P. Maattanen, and O. Øiseth, *Frequency domain force identification in ice-structure interaction*, in *The proceedings of the 22nd International Conference on Port and Ocean Engineering under Arctic Conditions*. 2013, Port and Ocean Engineering under Arctic Conditions.
[24] Bell, K., *An engineering approach to finite element analysis of linear structural mechanics problems*. 2013, Trondheim: Akademika Publ. XIX, 656 s. : ill.
[25] Haugen, B., *Buckling and Stability Problems for Thin Shell Structures Using High Performance Finite Elements*. 1994: University of Colorado.